Growth of Semiconducting Single-Walled Carbon Nanotubes Array by Precisely Inhibiting Metallic Tubes Using ZrO₂ Nanoparticles

*Dewu Lin, Yue Yu, Lanying Li, Mingzhi Zou, and Jin Zhang**

Synthesis of high-quality single-walled carbon nanotubes arrays with pure semiconducting type is crucial for the fabrication of integrated circuits in nanoscale. However, the naturally grown carbon nanotubes usually have diverse structures and properties. Here the bicomponent catalyst using Au and ZrO₂ is designed and prepared. The Au nanoparticle serves as the catalysts for carbon feedstock cracking and facilitating the nucleation of carbon nanotubes, whereas the close-connected ZrO₂ forms a localized etching zone around Au by releasing lattice oxygen and to inhibit the nucleation of metallic carbon nanotubes precisely. The obtained single-walled carbon nanotubes array show a high semiconducting content of >96%, on the basis of good performance of field-effect transistor devices. And such building of localized etching zone is compatible with other catalyst systems as a universal and efficient method for the scalable production of semiconducting carbon nanotubes.

The development of nanoelectronic devices based on single-walled carbon nanotubes (SWCNTs) requires the uniform structure of SWCNTs to show outstanding performance and reproducibility.[1] Even though the synthesis of single-chirality carbon nanotubes has made substantial progress,[2] it is still a long-standing goal to obtain mass-produced SWCNTs with pure chirality. Therefore, the scalable synthesis of electrical type-selected semiconducting SWCNTs (s-SWCNTs) is crucial and practical, and as for modern microprocessor and other electronic devices, s-SWCNTs have already shown the advantages over traditional silicon semiconductors.[3] Currently, there are two main approaches to achieve the enrichment of s-SWCNTs. The first one is postsynthesis sorting by chemical and physical treatments.[4] Although the high-purity (>99.99%)

Dr. D. W. Lin, Y. Yu, M. Z. Zou, Prof. J. Zhang
Center for Nanochemistry
Beijing Science and Engineering Center for Nanocarbons
Beijing National Laboratory for Molecular Sciences
College of Chemistry and Molecular Engineering
Peking University
Beijing 100871, P. R. China
E-mail: jinzhang@pku.edu.cn
L. Y. Li
China Bluestar Chengrand Chemical Co. Ltd.
4th Xinghua Road, Xinjin Industry Zone B, Chengdu 611430, P. R. China

s-SWCNTs have been obtained, drawbacks of structural damage and contamination are inevitable, let alone the high cost of complex processes and the environmentally unfriendly sacrifice of nanotubes.[5] The other way is direct growth in chemical vapor deposition (CVD) system, where the catalysts, gas flow, temperature, and substrate are essential factors for the structural control of SWCNTs. According to the principle that metallic SWCNTs (m-SWCNTs) are more chemically active than s-SWCNTs,[6] it has been popular to implement the strategy of in situ etching in the type-selective growth of s-SWCNTs, and various etching methods have been developed, like light irradiation,[7] ·H,[8] ·OH,[9] ·CH₃ radicals,[10] and H₂O,[6a] etc. Despite the respectable effort made with above methods, introducing etchant in the gas phase of CVD system will make it extremely difficult to achieve precise etching.[11] Because of the heterogeneous distribution of etchant in gas phase, the grown s-SWCNTs could be etched due to the adsorption of too much etchant, meanwhile, the nucleation of m-SWCNTs may escape from being inhibited. Therefore, it is more desirable to directly grow s-SWCNTs with purposeful structural control and scalable production by an advanced method.[12]

As for the catalytic growth of each carbon nanotubes, the nucleation of cap structure and addition of carbon atoms during growth both occurs at the surface of catalyst particles, so design of catalysts would be an efficient strategy to enable the structural control of SWCNTs.[13] Thus, confining the etching reaction to the site of nanotubes nucleation by the design of catalysts would make the inhibition of metallic tubes precise and harmless.

Metal oxide nanoparticles, which are able to store and release oxygen, are usually used as the exhaust gas purification three-way catalyst.[14] Especially for zirconia,[15] titania,[16] and ceria,[17] etc., such metal oxide nanoparticles are thermal stable at high temperature, and will release the stored lattice oxygen during the SWCNTs growth environment. When active catalysts of growing SWCNTs are combined with such metal oxide nanoparticles, the nucleation of SWCNTs could be surely selected by the surrounding lattice oxygen.

Here in this study, we report the design of bicomponent Au@ZrO₂ catalysts, which could achieve the direct growth of high-quality s-SWCNT arrays. Au particles with low melting point migrate easily at high temperature, whereas the ZrO₂
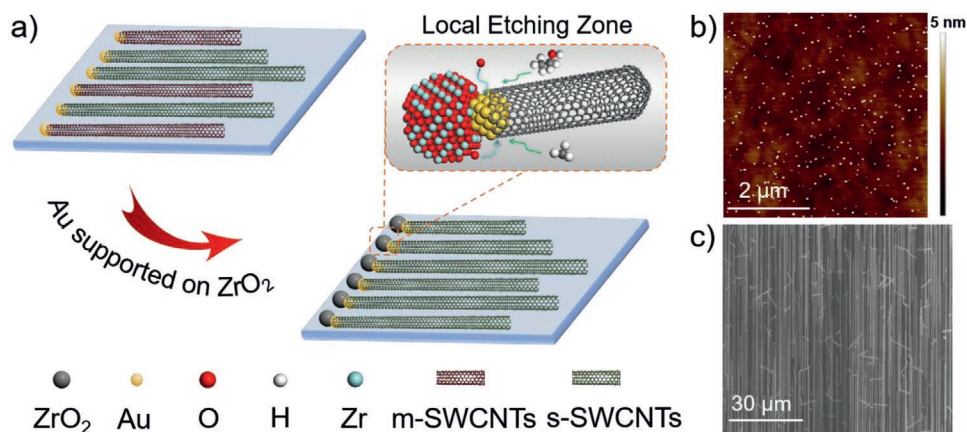
Figure 1. Direct growth of s-SWCNTs from Au particles supported on ZrO$_2$. a) Schematic showing the growth of s-SWCNTs from Au@ZrO$_2$ assisted by the localized etching zone. b) AFM image of the deposited Au@ZrO$_2$ catalysts. c) Typical SEM image of the as-obtained SWCNT horizontal array.

particles possess much higher melting point and would contribute to the anchoring of catalysts, and the tight binding between Au and ZrO$_2$ would be formed subsequently. Then, in the nanotubes growth environment, the releasing of lattice oxygen from ZrO$_2$ helps build a confined etching atmosphere to inhibit the nucleation of m-SWCNTs at the initial state. **Figure 1**a schematically illustrates the developed result of carbon nanotubes grown from Au@ZrO$_2$ catalysts when compared to individual Au catalysts. Details of the synthesis process are described in the Supporting Information. In brief, single side polished ST-cut quartz was used as the substrate to grow SWCNT arrays, and carbon nanotubes grown from Au particles were natural with 1/3 metallic ones, while the combination of ZrO$_2$ with Au promoted the building of localized etching zone next to the catalyst particles by releasing oxygen during growth, so that the m-SWCNT arrays could be etched initially. Figure 1b shows the atomic force microscopy (AFM) image of

the Au@ZrO$_2$ catalysts. The nanoparticles were well-dispersed and uniformly distributed on the quartz substrate. Sizes of 150 nanoparticles were measured using AFM, and the corresponding distribution is shown in Figure S1 (Supporting Information). Apparently, more than 90% Au@ZrO$_2$ catalysts were 2–7 nm in diameter, with an average diameter of 4.6 nm. Due to the combination with ZrO$_2$ nanoparticles as supporters, such size of Au@ZrO$_2$ catalyst is relatively larger than those reported metal catalysts of growing s-SWCNTs. The dispersion of catalysts are critical for the growth of SWCNT arrays, scanning electron microscope (SEM) image (Figure 1c) shows that a majority of carbon nanotubes with length longer than 30 µm are aligned horizontally, while few short SWCNTs (<10 µm) grew randomly.

Raman spectrometry is an effective method for the electrical type analysis of SWCNTs. To further confirm the selectivity of s-SWCNTs in our samples, two excitation lasers (wavelength of 532 and 633 nm) were used. **Figure 2**a,b,d,e shows the typical
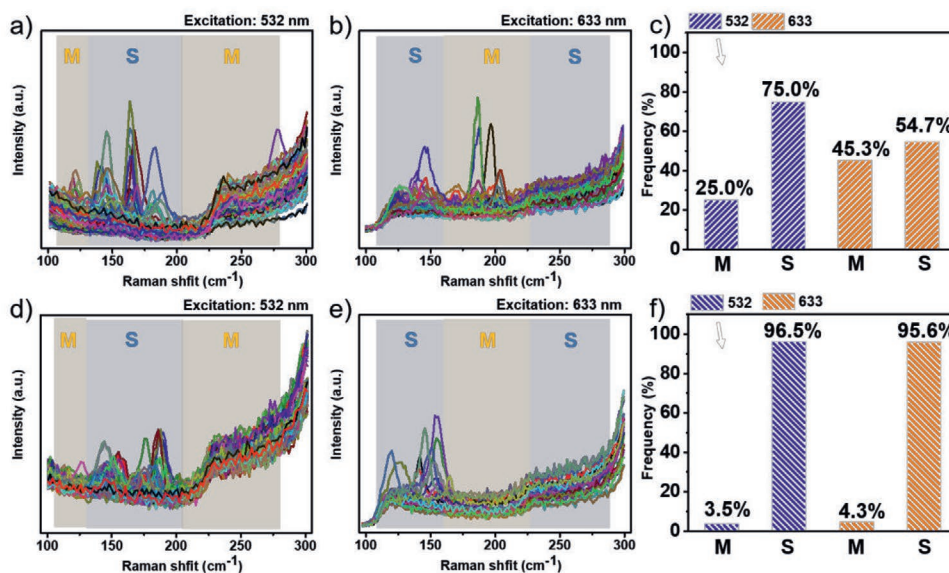

Figure 2. Electrical types of SWCNT arrays characterized by the multiwavelength Raman spectroscopy. a–c) RBM peaks of Raman spectra and corresponding statistical result of SWCNT arrays based on Au catalysts; d–f) RBM peaks of Raman spectra and corresponding statistical result of SWCNT arrays based on Au@ZrO$_2$ catalysts.

**ADVANCED
SCIENCE NEWS**
www.advancedsciencenews.com

NANO · MICRO
small
www.small-journal.com

radical breathing mode (RBM) peaks of Raman spectra, where the m- and s-SWCNTs were identified according to the Kataura plot.[18] Although dispersive Au nanoparticles could be obtained on quartz substrate with an average diameter of 3.4 nm, and enable the growth of SWCNTs array (Figure S2, Supporting Information), it is apparent that abundant m- and s-SWCNTs were both observed in the SWCNT arrays grown from Au catalysts (Figure 2a,b). While the m-SWCNTs were barely detected in the samples grown from Au@ZrO$_2$ catalysts (Figure 2d,e). The resultant content of s-SWCNTs is shown in Figure 2c,f, SWCNTs grown from Au possessed 75% semiconducting ones with 532 nm excitation laser and 55% with 633 nm excitation laser. As for the Au@ZrO$_2$ catalysts, there were >96% semiconducting ones with 532 nm excitation laser and >95% with 633 nm excitation laser. The respective numbers are recorded in Table S1 (Supporting Information), specifically, 92 of 137 (≈67%) SWCNTs grown from Au catalysts were identified as semiconducting, but 104 of 108 (>96%) were s-SWCNTs when Au@ZrO$_2$ catalysts were used. In addition, the G bands in Raman spectra of SWCNTs grown from Au@ZrO$_2$ catalysts (Figure S3, Supporting Information) show the obvious Lorenz shape,[19] which indicates the characteristic of s-SWCNTs, and the negligible D bands show the high quality of as-obtained SWCNT arrays as well.

In a common SWCNTs synthesis process, the metal catalyst precursors are usually calcined in air, and followed by the reduction procedure in hydrogen before the carbon feed stocks are introduced. As for Au@ZrO$_2$ catalysts, the selectivity of s-SWCNTs was attributed to the localized etching zone around the carbon nanotube nucleation sites. Thus, the prolongation of catalysts prereduction duration in hydrogen would decrease the content of released lattice oxygen and reduce the selectivity of s-SWCNTs. To investigate the role of the lattice oxygen, a typical control experiment was performed. As shown in Figure S4 (Supporting Information), when the reduction time was extended from 2 to 15 min, content of s-SWCNTs significantly decreased from 96% to 74%, and further decreased to 71% after 30 min reduction. X-ray photoelectron spectroscopy was used to characterize the valance state of zirconia. The Zr 3d electron region (Figure S5, Supporting Information) of the Au@ZrO$_2$ catalysts reduced in hydrogen for only 2 min shows two peaks at 182.4 and 184.8 eV, corresponding to $3d_{5/2}$ and $3d_{3/2}$ of Zr, and no apparent reduced state of zirconia was detected. After 30 min hydrogen reduction, another set of peaks (180.3 and 183.1 eV) appeared, which are attributed to the oxygen-deficient phase of zirconia, but metallic Zr (178.9 eV) was still absent. Therefore, above results indicate that reduction for long duration would cause the losing of lattice oxygen in ZrO$_2$, thereby reducing the selectivity of s-SWCNTs.

The selective synthesis of s-SWCNTs arrays was achieved by introducing ZrO$_2$ nanoparticles as the supporters of Au catalysts, further investigation of the catalyst structure would help to understand the way it worked. Thus, detailed transmission electron microscopy (TEM) characterization was performed. **Figure 3**a,c clearly shows that the small dark gray nanoparticles would always attach to the larger light gray ones. Typical atomic
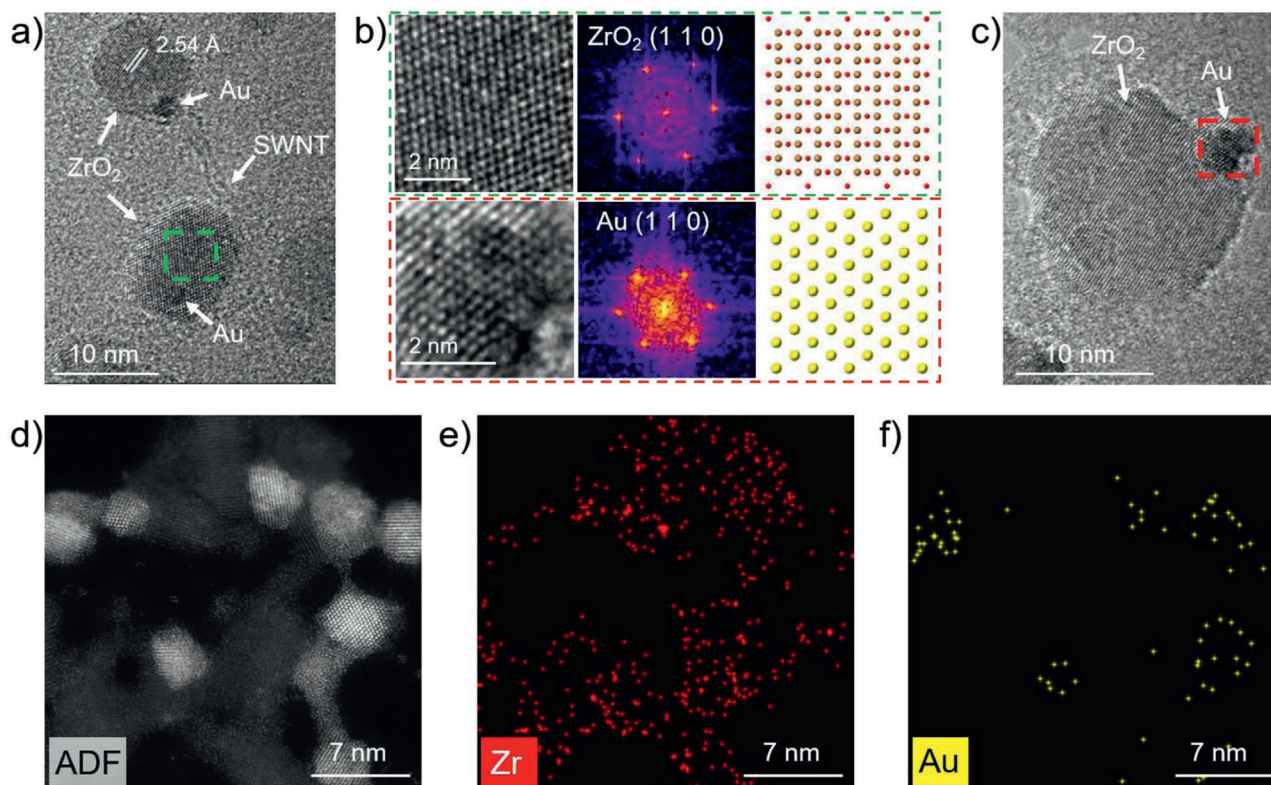

Figure 3. Characterization of Au@ZrO$_2$ catalysts. a) High-resolution TEM image of an individual SWCNT grown from the Au@ZrO$_2$ catalyst. b) Zoom-in TEM images, corresponding FFT of the nanoparticles and atomic structure models in a) (green dotted box) and c) (red dotted box). c) High-resolution TEM image of Au catalyst supported on ZrO$_2$. d) ADF-STEM image and e,f) EDS mapping images of Au@ZrO$_2$ catalysts.

ADVANCED
SCIENCE NEWS
www.advancedsciencenews.com

NANO · MICRO
small
www.small-journal.com

structures of the catalysts are shown in Figure 3b. According to the calculated fast Fourier transform (FFT) diffractogram, the atomic structures of light gray particles and dark gray particles are consistent with fcc ZrO_2 (1 1 0) and fcc Au (1 1 0), respectively. Figure 3d presents the annular dark field scanning transmission electron microscopy (ADF-STEM) image of Au@ZrO_2 catalysts on SiN_x grid, together with the energy-dispersive X-ray spectroscopy (EDS) mapping in Figure 3e,f, the structure morphology of zirconia loaded with Au nanoparticles was clearly revealed. EDS mapping confirmed that the white contrast particles in the ADF-STEM image (corresponding to the dark gray parts in high resolution TEM images) are Au, while the particles in darker contrast are ZrO_2. Linear mapping characterization (Figure S6, Supporting Information) also proves that such catalysts are composed of zirconia and gold particles.

After the nanotubes growth process, SWCNTs grown from the ZrO_2 supported Au nanoparticles were clearly observed (Figure 3a; and Figure S7, Supporting Information). Both ZrO_2 and Au nanoparticles could enable the catalytic growth of SWCNTs in appropriate condition, while Au undoubtedly possessed higher reactivity in our system.[20] The identification of catalyst structure after SWCNTs growth indicated that ZrO_2 nanoparticles were not the direct nucleation sites of SWCNTs but were indispensable for the selectively synthesis of s-SWCNT arrays. In addition, the interfacial misfit dislocation, generally formed when different nanoparticles crystallize and grow simultaneously, was observed between Au and ZrO_2 nanoparticles

(Figure S8, Supporting Information).[21] That dislocation indicates the close connection between Au and ZrO_2 nanoparticles, which would enhance the selective growth of SWCNTs by fast transfer of released oxygen from ZrO_2 to Au. And other carbon nanotubes were then prevented from being damaged.

Electrical measurement of field-effect transistors (FET) fabricated by SWCNTs can provide the direct evidence about the selectivity of s-SWCNT arrays (for more preparation details, see the Supporting Information). **Figure 4**a shows the optical and SEM images of fabricated FET device with a channel length of 6 µm and width of 45 µm, and there were dozens of SWCNTs serving as the channel material in each transistor. Typical transfer characteristic (I_{ds}–V_{ds}) in Figure 4b shows the I_{on}/I_{off} ratio higher than 10^3, indicating a high purity of s-SWCNTs. And more transfer characteristics were shown in Figure S9 (Supporting Information). All 73 FET devices based on SWCNT arrays grown from Au@ZrO_2 catalysts (Au@ZrO_2-FETs) had been measured, the corresponding I_{on}/I_{off} ratios were plotted in Figure 4c. Apparently, more than 90% of devices had the I_{on}/I_{off} ratios larger than 10, indicating the high enrichment of s-SWCNTs.[22] However, as for the SWCNT arrays grown from Au catalyst, their FET devices (Au-FETs) showed the I_{on}/I_{off} ratios less than 4, suggesting the mixing of s- and m-SWCNTs in the samples. Furthermore, on the basis of the I_{on}/I_{off} ratios of Au-FETs and the content of s-SWCNTs (Figure 2c) grown from Au catalysts, the mean conductance ratio of m-SWCNTs to s-SWCNTs in our obtained samples was calculated to be 1.6 (for more details, see the description
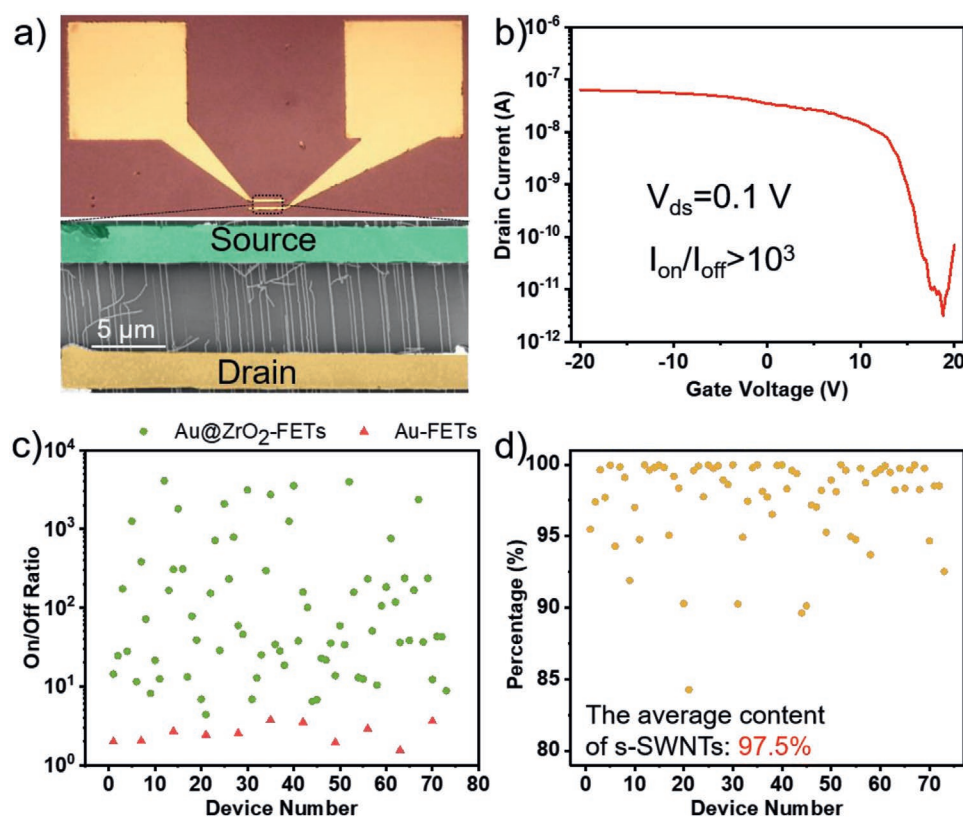

Figure 4. Electrical characterization of s-SWCNTs FETs. a) Optical (upper) and SEM (lower) images of the typical SWCNTs FET device, W_{ch} = 45 µm, L_{ch} = 6 µm. b) Typical transfer characteristic of the SWCNT FET device. c) The statistical result of I_{on}/I_{off} ratios based on each FET devices. d) Corresponding statistical result of the semiconducting SWCNTs' purity.

ADVANCED
SCIENCE NEWS
www.advancedsciencenews.com

NANO · MICRO
small
www.small-journal.com

of Figure S10, Supporting Information).[23] According to this result, the content of s-SWCNTs in each Au@ZrO$_2$-FET were calculated and plotted in Figure 4d, nearly all the FETs possess more than 90% semiconducting tubes, the average content of s-SWCNTs was 97.5%, which was consistent with the result of Raman characterization (Figure 2f).

Due to the formation of localized etching zone with ZrO$_2$, it is promising for other catalyst particles, such as transition metal particles, to grow s-SWCNTs directly when loaded on ZrO$_2$. Therefore, Cu@ZrO$_2$ and Fe@ZrO$_2$ catalysts were prepared by the same method, and applied for the synthesis of s-SWCNTs. Figure S11a,d shows (Supporting Information) the typical SEM images of SWCNT arrays grown from Cu@ZrO$_2$ and Fe@ZrO$_2$ catalysts, respectively. Obviously, the introduction of ZrO$_2$ supporters would not affect the alignment of SWCNT arrays. Subsequent Raman spectroscopy analysis showed that there were >88% (91 of 103) s-SWCNTs in the sample grown from Cu@ZrO$_2$, and >88% (89 of 101) s-SWCNTs for Fe@ZrO$_2$ catalysts. Considering that the synthesis parameters have not been optimized, the higher selectivity of s-SWCNTs could be expected soon.

To summarize, bicomponent Au@ZrO$_2$ catalysts were designed for the selective growth of s-SWCNTs. Oxygen storing-releasing ability of zirconia was utilized to build the localized etching zone next to the catalytic Au particles, so that the nucleation of m-SWCNTs was inhibited initially. Benefit from the precise location of etching zone, the etching damage to nanotubes could be avoided as well. It was noted that high-quality SWCNT arrays with >96% semiconducting content were obtained. And such building of localized etching zone is compatible with other catalyst systems as a universal and efficient method for the scalable production of semiconducting carbon nanotubes.

Supporting Information

Supporting Information is available from the Wiley Online Library or from the author.

Conflict of Interest

The authors declare no conflict of interest.

Keywords

etching, lattice oxygen, semiconducting carbon nanotubes, zirconia

[1] a) R. Saito, M. Fujita, G. Dresselhaus, M. S. Dresselhaus, *Appl. Phys. Lett.* **1992**, *60*, 2204; b) S. J. Tans, A. R. M. Verschueren, C. Dekker, *Nature* **1998**, *393*, 49; c) A. Javey, J. Guo, Q. Wang, M. Lundstrom, H. Dai, *Nature* **2003**, *424*, 654.

[2] a) F. Yang, X. Wang, D. Zhang, J. Yang, D. Luo, Z. Xu, J. Wei, J.-Q. Wang, Z. Xu, F. Peng, X. Li, R. Li, Y. Li, M. Li, X. Bai, F. Ding, Y. Li, *Nature* **2014**, *510*, 522; b) Q. Zhao, Z. Xu, Y. Hu, F. Ding, J. Zhang, *Sci. Adv.* **2016**, *2*, e1501729; c) S. Zhang, L. Kang, X. Wang, L. Tong, L. Yang, Z. Wang, K. Qi, S. Deng, Q. Li, X. Bai, F. Ding, J. Zhang, *Nature* **2017**, *543*, 234.

[3] a) A. D. Franklin, *Nature* **2013**, *498*, 443; b) M. M. Shulaker, G. Hills, N. Patil, H. Wei, H.-Y. Chen, H. S. P. Wong, S. Mitra, *Nature* **2013**, *501*, 526; c) M. M. Shulaker, J. Van Rethy, T. F. Wu, L. Suriyasena Liyanage, H. Wei, Z. Li, E. Pop, G. Gielen, H. S. P. Wong, S. Mitra, *ACS Nano* **2014**, *8*, 3434; d) G. J. Brady, A. J. Way, N. S. Safron, H. T. Evensen, P. Gopalan, M. S. Arnold, *Sci. Adv.* **2016**, *2*, e1601240; e) G. Hills, C. Lau, A. Wright, S. Fuller, M. D. Bishop, T. Srimani, P. Kanhaiya, R. Ho, A. Amer, Y. Stein, D. Murphy, A. C. Arvind, M. M. Shulaker, *Nature* **2019**, *572*, 595.

[4] a) H. Zhang, B. Wu, W. Hu, Y. Liu, *Chem. Soc. Rev.* **2011**, *40*, 1324; b) S. A. Hodge, M. K. Bayazit, K. S. Coleman, M. S. P. Shaffer, *Chem. Soc. Rev.* **2012**, *41*, 4409.

[5] X. Li, L. Zhang, X. Wang, I. Shimoyama, X. Sun, W.-S. Seo, H. Dai, *J. Am. Chem. Soc.* **2007**, *129*, 4890.

[6] a) W. Zhou, S. Zhan, L. Ding, J. Liu, *J. Am. Chem. Soc.* **2012**, *134*, 14019; b) B. Yu, C. Liu, P.-X. Hou, Y. Tian, S. Li, B. Liu, F. Li, E. I. Kauppinen, H.-M. Cheng, *J. Am. Chem. Soc.* **2011**, *133*, 5232; c) C. Liu, H.-M. Cheng, *J. Am. Chem. Soc.* **2016**, *138*, 6690.

[7] a) H. Huang, R. Maruyama, K. Noda, H. Kajiura, K. Kadono, *J. Phys. Chem. B* **2006**, *110*, 7316; b) G. Hong, B. Zhang, B. Peng, J. Zhang, W. M. Choi, J.-Y. Choi, J. M. Kim, Z. Liu, *J. Am. Chem. Soc.* **2009**, *131*, 14642.

[8] F. Zhang, P.-X. Hou, C. Liu, B.-W. Wang, H. Jiang, M.-L. Chen, D.-M. Sun, J.-C. Li, H.-T. Cong, E. I. Kauppinen, H.-M. Cheng, *Nat. Commun.* **2016**, *7*, 11160.

[9] a) L. Ding, A. Tselev, J. Wang, D. Yuan, H. Chu, T. P. McNicholas, Y. Li, J. Liu, *Nano Lett.* **2009**, *9*, 800; b) S. Zhang, Y. Hu, J. Wu, D. Liu, L. Kang, Q. Zhao, J. Zhang, *J. Am. Chem. Soc.* **2015**, *137*, 1012.

[10] G. Zhang, P. Qi, X. Wang, Y. Lu, X. Li, R. Tu, S. Bangsaruntip, D. Mann, L. Zhang, H. Dai, *Science* **2006**, *314*, 974.

[11] Q. Zhao, F. Yao, Z. Wang, S. Deng, L. Tong, K. Liu, J. Zhang, *Adv. Mater.* **2017**, *29*, 1701959.

[12] a) X. Qin, F. Peng, F. Yang, X. He, H. Huang, D. Luo, J. Yang, S. Wang, H. Liu, L. Peng, Y. Li, *Nano Lett.* **2014**, *14*, 512; b) L. Kang, S. Zhang, Q. Li, J. Zhang, *J. Am. Chem. Soc.* **2016**, *138*, 6727.

[13] Y. Li, R. Cui, L. Ding, Y. Liu, W. Zhou, Y. Zhang, Z. Jin, F. Peng, J. Liu, *Adv. Mater.* **2010**, *22*, 1508.

[14] a) E. Bekyarova, P. Fornasiero, J. Kašpar, M. Graziani, *Catal. Today* **1998**, *45*, 179; b) Z. M. Shi, Y. Liu, W. Y. Yang, K. M. Liang, F. Pan, S. R. Gu, *J. Eur. Ceram. Soc.* **2002**, *22*, 1251.

[15] A. Sinhamahapatra, J.-P. Jeon, J. Kang, B. Han, J.-S. Yu, *Sci. Rep.* **2016**, *6*, 27218.

[16] X. Chen, L. Liu, P. Y. Yu, S. S. Mao, *Science* **2011**, *331*, 746.

[17] C. T. Campbell, C. H. F. Peden, *Science* **2005**, *309*, 713.

[18] H. Kataura, Y. Kumazawa, Y. Maniwa, I. Umezu, S. Suzuki, Y. Ohtsuka, Y. Achiba, *Synth. Met.* **1999**, *103*, 2555.

[19] A. Jorio, A. G. Souza Filho, G. Dresselhaus, M. S. Dresselhaus, A. K. Swan, M. S. Ünlü, B. B. Goldberg, M. A. Pimenta, J. H. Hafner, C. M. Lieber, R. Saito, *Phys. Rev. B* **2002**, *65*, 155412.

[20] S. Bhaviripudi, E. Mile, S. A. Steiner, A. T. Zare, M. S. Dresselhaus, A. M. Belcher, J. Kong, *J. Am. Chem. Soc.* **2007**, *129*, 1516.

[21] P. Bouvier, E. Djurado, G. Lucazeau, T. Le Bihan, *Phys. Rev. B* **2000**, *62*, 8731.

ADVANCED
SCIENCE NEWS

www.advancedsciencenews.com

NANO · MICRO

small

www.small-journal.com

[22] Y. Che, C. Wang, J. Liu, B. Liu, X. Lin, J. Parker, C. Beasley, H. S. P. Wong, C. Zhou, *ACS Nano* **2012**, *6*, 7454.

[23] a) A. E. Islam, F. Du, X. Ho, S. Hun Jin, S. Dunham, J. A. Rogers, *J. Appl. Phys.* **2012**, *111*, 054511; b) S. H. Jin, S. N. Dunham, J. Song, X. Xie, J.-h. Kim, C. Lu, A. Islam, F. Du, J. Kim, J. Felts, Y. Li, F. Xiong, M. A. Wahab, M. Menon, E. Cho, K. L. Grosse, D. J. Lee, H. U. Chung, E. Pop, M. A. Alam, W. P. King, Y. Huang, J. A. Rogers, *Nat. Nanotechnol.* **2013**, *8*, 347.

2006605 (6 of 6)